Struct Multidisc Optim (2014) 50:505–515
DOI 10.1007/s00158-014-1073-3

INDUSTRIAL APPLICATION

Conceptual and basic designs of the Mobile Harbor crane based on topology and shape optimization

In Gwun Jang · Kyung-Soo Kim · Byung Man Kwak

Received: 7 August 2013 / Revised: 21 January 2014 / Accepted: 14 February 2014 / Published online: 30 March 2014

Abstract The Mobile Harbor (MH) has been recently proposed as a novel maritime cargo transfer system that can move to a container ship anchored in the deep sea and handle containers directly at sea with the aid of a stabilized MH crane. Because this system operates under at-sea conditions, the MH crane must be designed to support an inertia load and wind force, as well as its self-weight. The wave-induced motions of the MH, e.g. rolling, pitching, and heaving, generate a significant amount of inertia load, which has not been considered in the design of conventional quayside cranes installed on stable ground. Wind force is also a critical design factor due to the higher wind velocity in the open sea. In addition to the aforementioned structural rigidity, mass minimization is also important in the structural design of MH cranes because it reduces the overturning moment and therefore enhances ship stability. In this paper, the sensitivities of the design-dependent loads (i.e. self-weight, inertia load, and wind force) are derived with respect to the design variables, and then a topology optimization is conducted with the derived sensitivities in order to obtain a conceptual design. Then, the conceptual design is elaborated into a three-dimensional basic design through shape optimization with design regulations for offshore cranes. Through the integrated design process with the topology and shape optimizations, a conceptual and basic design is successfully obtained for the MH crane.

Keywords Topology optimization · Shape optimization · Design-dependent load · Mobile Harbor · Offshore crane

I. G. Jang (✉)
The Cho Chun Shik Graduate School for Green Transportation, Korea Advanced Institute of Science and Technology, 373-1 Guseong-dong, Yuseong-gu, Daejeon 305-701, Republic of Korea
e-mail: jangin0407@kaist.ac.kr

K.-S. Kim · B. M. Kwak
Department of Mechanical Engineering, Korea Advanced Institute of Science and Technology, 373-1 Guseong-dong, Yuseong-gu, Daejeon 305-701, Republic of Korea

K.-S. Kim
e-mail: kyungsookim@kaist.ac.kr

B. M. Kwak
e-mail: bmkwak@kaist.ac.kr

1 Introduction

Because container shipping is important in worldwide trade, the quantity of goods transported by container ships increases every year. This has led to rapid increases in the size of container ships from 5,000 twenty-foot equivalent units (TEU) to over 10,000 TEU in order to achieve more efficient maritime logistics. The advent of such supersized container ships has prompted the need for enhanced capacity and capability at container ports because the existing ports have already reached their limitation in terms of facilities and drafts. Therefore, there is an urgent need for new port systems (or transfer systems) to be developed in order to effectively manage mega-sized container ships. In order to meet these societal and logistic demands, the concept of the Mobile Harbor (MH) (Kim et al. 2013, 2014) was recently proposed to directly load and unload containers from container ships anchored in the open sea, as shown in Fig. 1.

The significant technical challenge in developing the MH is to consider the environmental disturbances, such as waves and wind, under the operating conditions and survival conditions in both structural design and control.

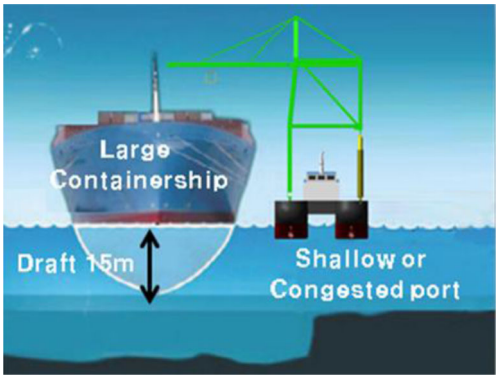

Fig. 1 Concept of mobile Harbor

Unlike conventional quayside cranes that are mounted on stable ground, MH cranes should be designed to support inertia loads and wind forces as well as its self-weight due to wave-induced motions, wind, and heavy weights. In addition to the structural rigidity under at-sea conditions, mass minimization is critical in the structural design because it generally reduces the overturning moment and therefore enhances ship stability.

Topology optimization can be utilized to obtain a conceptual design that satisfies the aforementioned features. Topology optimization is generally known to have a greater impact on the downstream of the design process because the topology should be determined prior to the size or shape. The literature features several methods of topology optimization: the homogenization method (Bendsoe and Kikuchi 1988; Hassani and Hinton 1998), the solid isotropic material with penalization (SIMP) method (Bendsoe 1989; Yang and Chuang 1994), the evolutionary structural optimization (ESO) method (Xie and Steven 1993; Querin et al. 1998), and the level set method (Osher and Sethian 1988; Wang et al. 2003). Design space optimization (Kim and Kwak 2002; Jang and Kwak 2006, 2008) was also developed using a mathematical derivation of the effect of the design space changes, i.e. the design space sensitivity. Its capability and efficiency were demonstrated through various numerical examples (Jang and Kim 2009, 2010). In most topology optimizations, however, it is assumed that the loads remain fixed in terms of location, magnitude, and direction (i.e. dead loads). Since 2000, many papers (Hammer and Olhoff 2000; Park et al. 2003; Bruyneel and Duysinx 2005; Du and Olhoff 2004a, b; Zhang et al. 2008) have addressed topology optimization with design-dependent loads (e.g. self-weight, inertia loads, and wind forces), and these design-dependent loads are critical for numerous structural cases such as the MH crane. Recently, Zakhama et al. (2010) proposed a wind load modeling based on the standard formula for drag forces and applied it to topology optimization. The difficulty of design-dependent loads is that the location, magnitude, and direction of the loads change as the shape of the structure changes.

This paper presents a conceptual design for Mobile Harbor cranes that operate under at-sea conditions and then elaborate the design through shape optimization with design regulations for offshore cranes. For this purpose, an isovolumetric contour was created using the shape functions in finite element analysis (FEA) in order to consider changes in the location of the wind force on the structure as a continuous function; then, the sensitivities of design-dependent loads were derived for topology optimization. After the conceptual design of the MH crane was successfully obtained using the topology optimization with the derived sensitivities, the shape optimization was conducted in order to determine the optimal dimensions of the cross sections that can satisfy the design criteria in the Korea Register of Shipping (KR) rulebook. This paper demonstrates that the conceptual and basic designs of the Mobile Harbor crane were obtained effectively through the systematic integration of the topology and shape optimization.

2 Topology optimization for conceptual design

In order to obtain a meaningful layout for a Mobile Harbor crane, all dominant loads in both operating and survival conditions must be considered: payload, self-weight, inertia load, and wind force. Except the container payload, all other loads are design-dependent; therefore, the magnitude, location, and direction of the loading are coupled to the structure layout. The following subsections describe the schemes in detail.

2.1 Sensitivity analysis

In this paper, the element-wise density and Young's modulus of the material (ρ_i and E_i, respectively) are simplified with the introduction of an element-wise volumetric usage (μ_i), as follows:

$$\rho_i = (\mu_i)\rho_0, \tag{1}$$

$$E_i = \begin{cases} \mu_i(\mu_{th})^{p-1}E_0, & \mu_{\min} \le \mu_i \le \mu_{th} \\ (\mu_i)^p E_0, & \mu_{th} < \mu_i \le 1 \end{cases}, \tag{2}$$

where ρ_0 and E_0 denote the base element density and Young's modulus, respectively, and p is a penalty number (3 in this paper). In (1), the element is regarded as a full solid with $\mu_i = 1$ and a void with $\mu_i = 0$. The element-wise volumetric usage (μ_i) is assumed to be constant in the element and is selected as a design variable. Note that instead of the typical solid isotropic material with penalization (SIMP) method, a modified SIMP with $\mu_{th} = 0.25$ was

used in (2) in order to avoid the numerical problems that occur in low densities due to the excessive ratio of mass to stiffness as Pedersen (2000) suggested. A small number for $\mu_{\min}$ (0.01 in this study) was used to prevent singularity in the finite element analysis. An alternative solution to avoid these numerical problems is to adopt a material interpolation scheme that delivers a moderate ratio in the low density region, such as the rational approximation for material properties (RAMP) method proposed by Stolpe and Svanberg (2001).

The basic formulation of this problem is the minimization of the compliance subject to a given volume fraction of the material. Incorporated with the finite element method and SIMP, the design domain is discretized into finite elements and the formulation becomes:

$$\begin{aligned} &minimize \;\; C = \mathbf{F}^T\mathbf{u} \\ &subject\ to \;\; \sum_{i=1}^{n} \mu_i V_i \le V_0 \\ &\qquad\qquad \mu_{\min} \le \mu_i \le 1 \quad i = 1, \cdots, n \end{aligned} \tag{3}$$

where $\mathbf{F}$ and $\mathbf{u}$ are the nodal load and nodal displacement vectors, respectively, and V_i is the volume (or area) of a finite element.

When a design-dependent load is considered, the sensitivity of compliance with respect to a design variable (Bruyneel and Duysinx 2005) becomes:

$$\frac{\partial C}{\partial \mu_i} = 2\mathbf{u}^T \frac{\partial \mathbf{F}}{\partial \mu_i} - \mathbf{u}^T \frac{\partial \mathbf{K}}{\partial \mu_i}\mathbf{u}, \tag{4}$$

where $\mathbf{K}$ is the stiffness matrix and it has a relationship of $\mathbf{Ku} = \mathbf{F}$. Note that design-independent loads such as payloads cause $\partial\mathbf{F}/\partial\mu_i$ to disappear. For the gravitational load (i.e. self-weight), if the gravity is applied along the $(-y)$ direction and a four-node plane element is used, the nodal gravitational load is as follows:

$$\mathbf{f}_g = \left\{ 0 \;\; -\mu_i \rho_0 \tfrac{V_i}{4} g \;\; \cdots \;\; 0 \;\; -\mu_i \rho_0 \tfrac{V_i}{4} g \right\}^T, \tag{5}$$

where g is the gravitational acceleration. If the heave motion of the Mobile Harbor (thus the $\pm y$ direction) due to waves is present, g in (5) should be modified to $g \pm a_h$ with the appropriate sign for the heave acceleration (a_h). If the angular acceleration of α_x, α_y, and α_z is assumed at the center of mass of the vessel regarding its rolling and pitching, the induced acceleration of the ith local node in the element due to rotation is derived as follows:

$$\begin{aligned} {}_i\mathbf{a}_r &= \boldsymbol{\alpha} \times \mathbf{r} \\ &= \begin{vmatrix} i & j & k \\ \alpha_x & \alpha_y & \alpha_z \\ x_i - x_o & y_i - y_o & z_i - z_o \end{vmatrix} \\ &= (\alpha_y(z_i - z_o) - \alpha_z(y_i - y_o), -\alpha_x(z_i - z_o) \\ &\quad + \alpha_z(x_i - x_o), \alpha_x(y_i - y_o) - \alpha_y(x_i - x_o)) \\ &= ({}_ia_x, {}_ia_y, {}_ia_z), \end{aligned} \tag{6}$$

where (x_i, y_i, z_i) and (x_0, y_0, z_0) denote the coordinates of the ith local node and center of rotation, respectively. In this paper, it is assumed that the center of rotation is located at the center of mass. Then, the nodal inertia load due to rotation for the four-node plane element becomes:

$$\begin{aligned} \mathbf{f}_r = \Big\{ &\mu_i \rho_0 \tfrac{V_i}{4}({}_1a_x) \;\; \mu_i \rho_0 \tfrac{V_i}{4}({}_1a_y) \;\; \cdots \;\; \mu_i \rho_0 \tfrac{V_i}{4}({}_4a_x) \\ &\mu_i \rho_0 \tfrac{V_i}{4}({}_4a_y) \Big\}^T. \end{aligned} \tag{7}$$

For nodal wind loads, a continuous surface representation is necessary for the domain where the wind loads act. This will be explained in Section 2.2 in detail. Once the nodal wind loads ($\mathbf{f}_w$) are obtained, the resultant nodal loads become:

$$\mathbf{f} = \mathbf{f}_p + \mathbf{f}_g + \mathbf{f}_r + \mathbf{f}_w, \tag{8}$$

where $\mathbf{f}_p$ denotes the payload. By assembling (8) and inserting it into (4), the sensitivity of the compliance is obtained with respect to a design variable.

2.2 Isovolumetric contour

Due to the discontinuity in its density distribution as shown in Fig. 2a, it is impossible to directly use SIMP to obtain wind loads and their sensitivities. Hammer and Olhoff (2000) proposed a smooth surface representation for static pressure loading. Similarly, in this paper, the nodal volume usage is calculated by averaging the volume usage of all elements sharing the node. If the same shape functions used in the elements are used here, a continuous field of volume usage ($\mu(x,y,z)$, see Fig. 2b) can be created as follows:

$$\mu(x, y, z) = \mathbf{N}^T \propto_n, \tag{9}$$

where $\propto_n$ is the nodal volume usage vector for the element and $\mathbf{N}$ is a shape function matrix of $m \times 1$, where m is the number of nodes in the element. Note that $\mathbf{N}$ has an individual shape function (N_i) for the ith node in the element as its ith component.

If a threshold value is selected for the isovolumetric surface (μ_c), then the exact contour where the wind loads act can be obtained by solving:

$$\mu(x, y, z) = \mu_c. \tag{10}$$

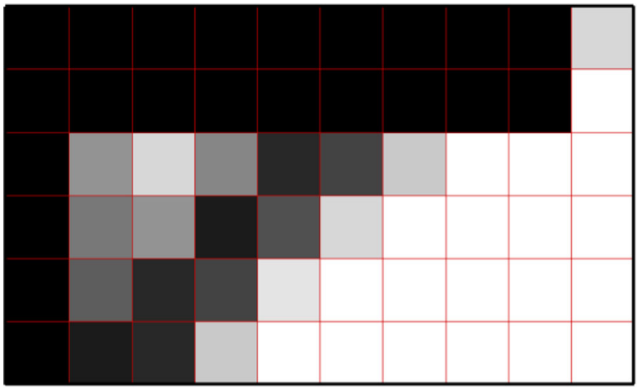

(a) Discrete distribution

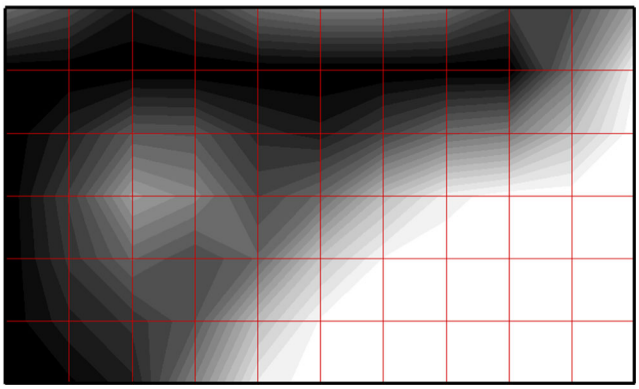

(b) Continuous distribution

Fig. 2 Comparison of discrete and continuous volume usage distributions

However, for simplicity, the intersection points on the element boundary are obtained from (10) and then the contour is approximated as a straight line in each element. In principle, the total wind load is proportional to the length of the isovolumetric line, which is in turn dependent on the selection of a threshold value. It should be noted that the conventional SIMP methods generate a grey zone between a solid (i.e. $\mu = 1$) and a void (i.e. $\mu = \mu_{\min}$). However, if the width of the grey zone is much smaller than the total length of the outermost boundary of the structure, the deviation of the length of the isovolumetric line due to variations of a threshold value may become negligible compared with the length of the isovolumetric line itself. This implies that the total wind load varies within an acceptable range. In the finite element method, consistent nodal loads that result from pressure can be calculated using:

$$\mathbf{r}_e = \int_S \mathbf{N}\boldsymbol{\Phi} dS, \tag{11}$$

where $\boldsymbol{\Phi}$ denotes a pressure vector on the surface (S). If the integration of wind pressure (p) along the straight line obtained above is considered (Fig. 3), the nodal wind load for a four-node plane element ($\mathbf{f}_w$) becomes:

$$\mathbf{f}_w = pt \int_{x_1}^{x_2} \mathbf{N}^T \left\{ \begin{matrix} -\frac{y_2 - y_1}{x_2 - x_1} \\ 1 \end{matrix} \right\} dx, \tag{12}$$

where (x_1,y_1) and (x_2,y_2) are two intersection points on the element boundary obtained from (10) and t is the element thickness. According to the Korea Register of Shipping (KR) rulebook (listed in the reference), the wind pressure (Pa in unit) on an offshore crane can be calculated by:

$$p = \frac{1}{16} C_h C_s g V^2, \tag{13}$$

where C_h and C_s denote the height factor and shape factor, respectively, and V is the wind velocity (m/s in unit). In this paper, a box girder is assumed to be the main structural member and $C_s = 1.6$ is used as the worst-case scenario. Detailed values for C_h are listed in Table 1. Figure 3 presents an example of the nodal wind loads on the isovolumetric contour of $\mu_c = 0.5$ when the wind blows in the $+x$ axis.

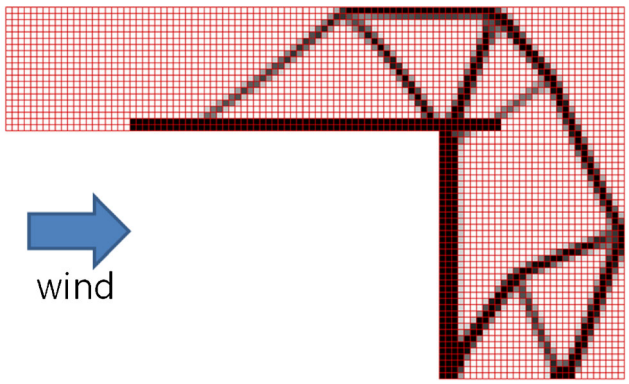

(a) Layout of the structure

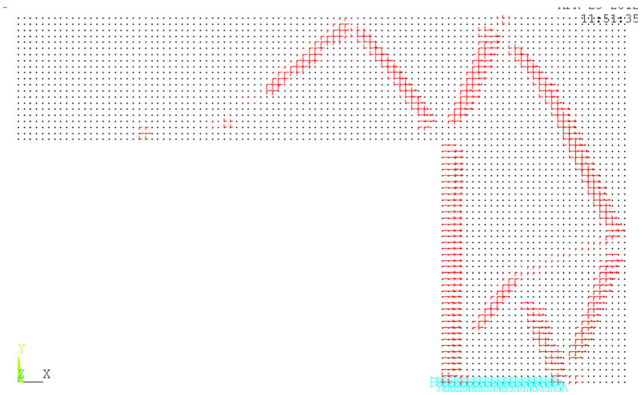

(b) Nodal wind load

Fig. 3 Example of nodal wind loads

Table 1 Height factor, C_h (KR rule book, listed in the reference)

Vertical height, h (m)	C_h
$h < 15.3$	1.00
$15.3 \leq h < 30.5$	1.10
$30.5 \leq h < 46.0$	1.20
$46.0 \leq h < 61.0$	1.30
$61.0 \leq h < 76.0$	1.37
$76.0 \leq h$	Value as considered appropriate by the Society

Because $\mathbf{f}_w$ is a function of intersection points, i.e. (x_i, y_i), as expressed in (12), $\partial \mathbf{f}_w / \partial \mu_i$ in the 2D case can be expressed as follows:

$$\frac{\partial \mathbf{f}_w}{\partial \mu_i} = \frac{\partial \mathbf{f}_w}{\partial x_1}\frac{\partial x_1}{\partial \mu_i} + \frac{\partial \mathbf{f}_w}{\partial y_1}\frac{\partial y_1}{\partial \mu_i} + \frac{\partial \mathbf{f}_w}{\partial x_2}\frac{\partial x_2}{\partial \mu_i} + \frac{\partial \mathbf{f}_w}{\partial y_2}\frac{\partial y_2}{\partial \mu_i}. \quad (14)$$

Note that the coordinates of the intersection points can be expressed with nodal volume usages using a symbolic operation, and these "nodal" volume usage are a function of the "element-wise" volume usage (μ_i). Then, from (12), $\partial \mathbf{f}_w / \partial x_1$, $\partial \mathbf{f}_w / \partial y_1$, $\partial \mathbf{f}_w / \partial x_2$, and $\partial \mathbf{f}_w / \partial y_2$ can be obtained; then, $\partial \mathbf{f}_w / \partial \mu_i$ can be calculated in the 2D case based on the isovolumetric representation.

In order to verify sensitivities of nodal wind loads from (14), four case studies were conducted: a vertical case, a horizontal case, a 45° inclined case, and an arbitrary case as shown Fig. 4. In all cases, the center elements are of interest and the red dotted lines represent their isovolumetric lines of $\mu_c = 0.5$ with their nodal volume usages written. It was assumed that the wind blows in the $+x$ direction. Table 2 demonstrates that the proposed scheme provides accurate sensitivities compared with those from the Finite Difference Method (FDM) with a 0.1 % perturbation. When deriving the wind loads and their sensitivities in this paper, the shape functions of a bilinear quadrilateral element were used and the isovolumetric contour was approximated as a straight line in each element. Therefore, if a linear isovolumetric contour exists in the element, accurate values of wind loads and their sensitivities can be obtained. Conversely, if a nonlinear contour is present, a certain amount of accuracy may be lost. One simple remedy for accuracy is to increase the mesh resolution in order to make the isovolumetric contour in each element uniform (or linear).

2.3 Conceptual design for Mobile Harbor

In order to set an appropriate design domain, the dimensions of a target container ship and the Mobile Harbor were considered; thus, the red rectangle in Fig. 5a was chosen as the design domain. Furthermore, the necessity of a crane boom to transport containers from the container side to the Mobile Harbor side, and vice versa, was considered. Considering these points, the initial design domain was determined with a passive domain for the crane boom as shown with the coordinate system in Fig. 5b. It is assumed that the geometric boundary condition is fixed on the bottom of the initial design domain (i.e. $y = 0$ in Fig. 5b).

The operating conditions for the Mobile Harbor were set to the World Meteorological Organization (WMO) Sea State 3. Under this condition, one of the collaborative research teams conducted a ship motion analysis using WAMIT and WINPOST; 2.26 m/s^2, 0.197 rad/s^2, and 0.111 rad/s^2 were obtained as the maximum heave, roll, and pitch motions, respectively, at the center of mass of the Mobile Harbor. Then, these values were used to obtain the gravitational loads and inertia loads from (5) and (6), respectively. Furthermore, 7.5 m/s and 51.5 m/s were used as the wind velocities under operating and survival conditions from the KR rulebook (listed in the reference) in order to obtain the wind loads from (12) and (13).

For the Mobile Harbor, the following four load cases were used:

- Case 1: (payload 130.5 tons at the tip of a boom) + (roll 0.197 rad/s^2) + (heave 2.26 m/s^2) + head wind (7.5 m/s)
- Case 2: (payload 130.5 tons at the end of a boom) + (roll 0.197 rad/s^2) + (heave 2.26 m/s^2) + head wind (7.5 m/s)
- Case 3: (roll 0.197 rad/s^2) + (heave 2.26 m/s^2) + head wind (51.5 m/s)
- Case 4: (roll 0.197 rad/s^2) + (heave 2.26 m/s^2) + tail wind (51.5 m/s)

In Cases 1 and 2, the payload is derived under the assumption of

$$\begin{aligned} payload(ton) = \{&40(40ft\ container) + 15(spreader) \\ &+ 20(trolley)\} \times 1.45(impact\ factor) \\ &\times 1.2(dynamic\ factor). \end{aligned} \quad (15)$$

The final formulation for the topology optimization is given as follows:

$$\begin{aligned} &minimize \sum_{j=1}^{4} c_j \boldsymbol{F}_j^T \boldsymbol{u}_j \\ &subject\ to \sum_{i=1}^{n} \mu_i V_i \leq V_0 \\ &\mu_{\min} \leq \mu_i \leq 1 \quad i = 1, \cdots, n \end{aligned} \quad (16)$$

where c_j is the weighting factor and, in this paper, the same value of 0.25 was used for each load case.

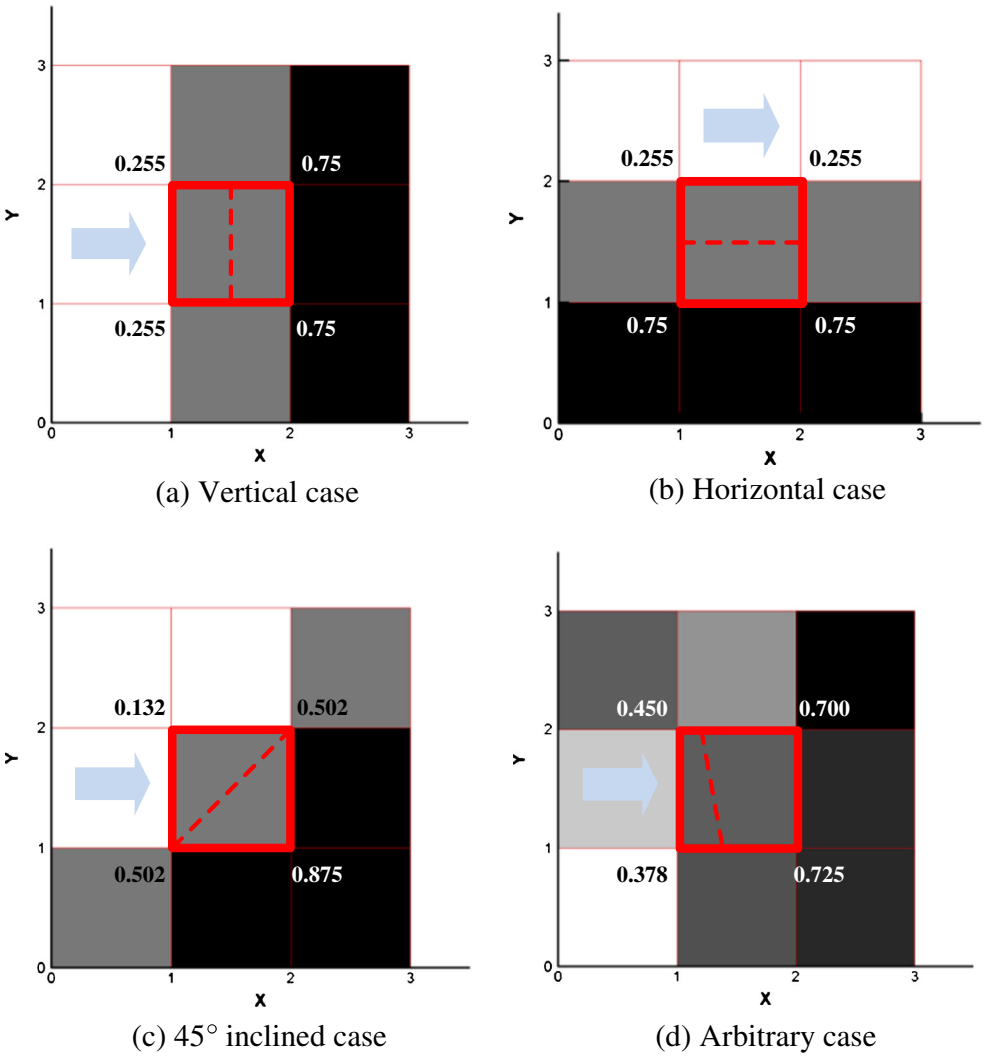

(a) Vertical case (b) Horizontal case

(c) 45° inclined case (d) Arbitrary case

Fig. 4 Verification examples for sensitivities of nodal wind loads

A two-dimensional FEA was performed using the commercial FEA package ANSYS. PLANE182 from the element library was used with the extra displacement shape option in order to avoid excessive shear stiffness (or so-called locking phenomena) in bending. For the optimization, the globally convergent method of moving asymptotes (GCMMA), which was proposed by Svanberg (2002), was used. This algorithm was chosen because it can provide non-monotonous approximations for design-dependent load problems. The optimization process was terminated when the maximum variation of the design variables over two successive iterations was less than 0.01. The optimization converged in 227 iterations through the convergence history shown in Fig. 6a and it took 132 min with Intel Core i7-950 CPU 3.07 GHz. It should be noted that, unlike typical compliance minimization problems with dead loads, the sensitivities of the compliance in (4) are not always negative and therefore compliance does not have a monotonous character with respect to the design variables. This property results in a significant difficulty in searching for the optimum. Figure 6b presents the conceptual layout for the Mobile Harbor crane considering the payload, self-weight, inertia load, and wind load.

3 Shape optimization for basic design

In this section, the conceptual design obtained in Section 2 is elaborated through shape optimization with detailed design regulations for offshore cranes. Such integrated design framework of the topology and shape optimization has been applied to structural design in aeronautics (Krog et al. 2002; James 2012).

In the first step, the basic design was reconstructed in 3D (Fig. 7) from the original 2D conceptual design. The

Table 2 Comparison of sensitivities of nodal wind loads

Case	Derived sensitivities	Sensitivities from FDM (with 0.1 % perturbation)	Accuracy(%)
Vertical	−1.0360000E-01	−1.0356368E-01	99.96
	1.0360000E-01	1.0356368E-01	99.96
	−1.0214000E-01	−1.0217357E-01	100.03
	1.0214000E-01	1.0217357E-01	100.03
	−1.0360000E-01	−1.0356368E-01	99.96
	1.0360000E-01	1.0356368E-01	99.96
	1.0214000E-01	1.0216411E-01	100.02
	−1.0214000E-01	−1.0216411E-01	100.02
Horizontal	0	0	100.00
	0	0	100.00
	0	0	100.00
	0	0	100.00
	0	0	100.00
	0	0	100.00
	0	0	100.00
	0	0	100.00
45° inclined	−1.0360000E-01	−1.0356368E-01	99.96
	1.0360000E-01	1.0356368E-01	99.96
	−1.0214000E-01	−1.0217357E-01	100.03
	1.0214000E-01	1.0217357E-01	100.03
	−1.0360000E-01	−1.0356368E-01	99.96
	1.0360000E-01	1.0356368E-01	99.96
	1.0214000E-01	1.0216411E-01	100.02
	−1.0214000E-01	−1.0216411E-01	100.02
Arbitrary	2.2600000E-01	2.4355437E-01	107.77
	9.3200000E-02	9.5846346E-02	102.84
	−2.5110000E-01	−2.4355437E-01	96.99
	−1.2983333E-02	−1.1787749E-02	90.79
	−2.7783333E-01	−2.7157391E-01	97.75
	−2.1333333E-02	−2.0334717E-02	95.32
	2.5283333E-01	2.7157391E-01	107.41
	1.0156667E-01	1.0439331E-01	102.78

foremost principle of reconstructing a conceptual design is to maintain the original load paths as much as possible and to reinforce the structure with additional structural members, if necessary. Through a literature survey of as-built drawings of conventional cranes and discussion with field experts, additional forestay links, backstay links, and a portal beam were included. In general, the forestay and backstay links prevent excessive deflection of the boom during cargo transfers, and a portal beam is essential in providing additional structural rigidity and therefore maintaining the rail span under various loads. The structural members of the crane were represented as beam and link elements with a predetermined set of cross sections (hollow rectangles and tubes for beam elements; solid circles for link elements) and relevant dimensions. Note that in the FE model, the link elements were used as tension-only members to represent the structural behavior of hanging cables, forestay links, and backstay links. Nonlinear FEA was conducted for large displacement. Heavy non-structural members such as a machinery house were also considered because these have a significant effect on the inertia loads.

An offshore crane should satisfy the design regulations in order to guarantee its safety in service and survival conditions in the open sea. In this paper, the Korea Register of Shipping (KR) rules were used as the design

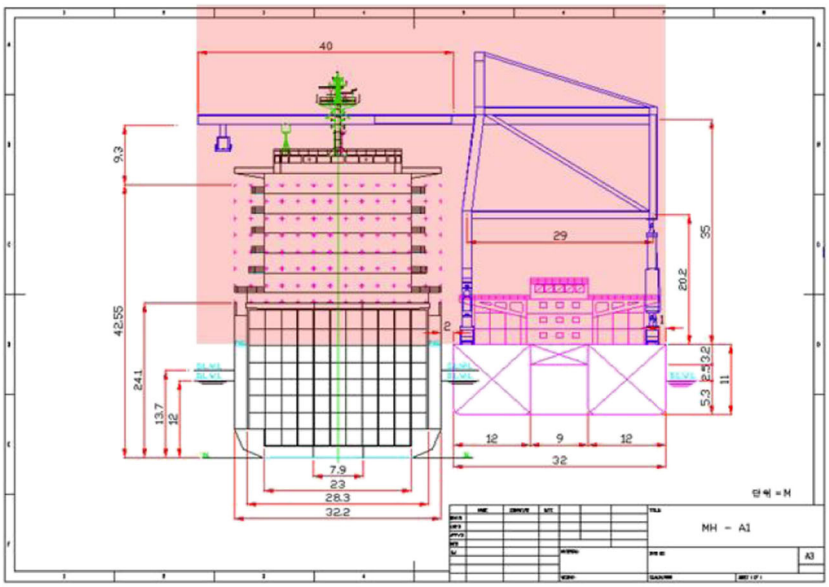

(a) Dimensions of a target container ship and the Mobile Harbor

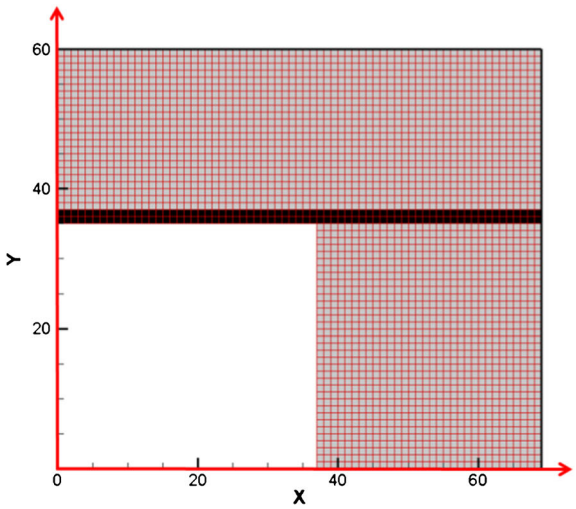

(b) Initial design domain of the Mobile Harbor

Fig. 5 Dimension and design domain of the Mobile Harbor

regulations. For the maximum allowable stress, 0.77 σ_Y was specified for the operating condition and 1.00 σ_Y for the survival condition, where σ_Y is the yield stress of a given material. For the members subjected to compression, the allowable compressive stress should be verified as a measure of buckling strength using the following equation:

$$\omega\sigma_c, \tag{17}$$

where σ_c is the axial compressive stress and ω can be calculated using the formula listed in Table 3. The detailed regulations are presented in the KR rulebook (listed in the reference).

Considering all the aforementioned regulations with (17), the new formulation for shape optimization is given as follows:

$$\begin{aligned} &minimize \ \sum_{i=1}^{n} m_i \\ &subject\ to\ \sigma_{eqv,i} \le \begin{cases} 0.77\sigma_Y & in\ operating\ condition \\ 1.00\sigma_Y & in\ survival\ condition \end{cases} \\ &\omega_i\sigma_{c,i} \le \begin{cases} 0.77\sigma_Y & in\ operating\ condition \\ 1.00\sigma_Y & in\ survival\ condition \end{cases} \\ &x_{lb,i} \le x_i \le x_{ub,i}, \quad i = 1, \cdots, 73 \end{aligned} \tag{18}$$

where m_i is the mass of the ith structural member, and $\sigma_{eqv,i}$ and $\sigma_{c,i}$ denote von Mises equivalent stress and

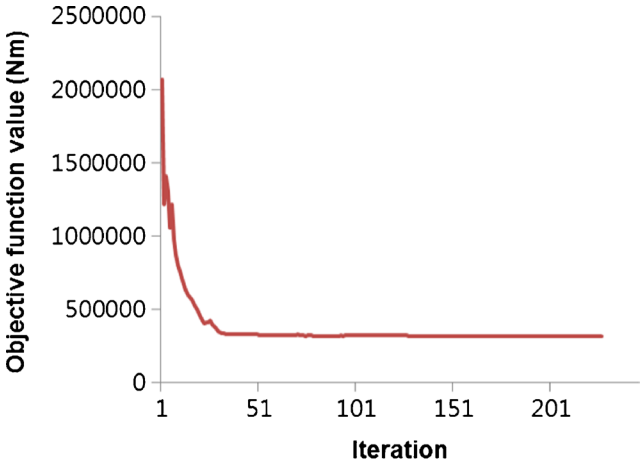

(a) Convergence history

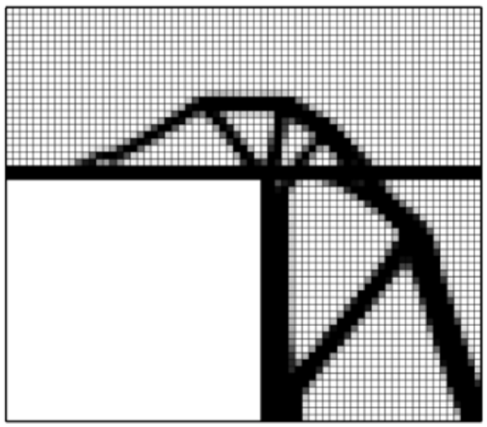

(b) Final result

Fig. 6 Optimization history and result of topology optimization

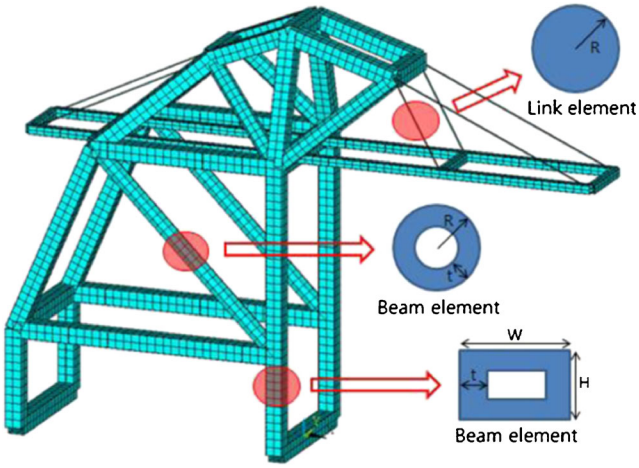

Fig. 7 Reconstructed basic design with cross-sectional design variables

Table 3 Formula for ω

Relation between λ and λ_0	Type of members	Formula for ω
$\lambda \geq \lambda_0$	All members	$2.9\left(\frac{\lambda}{\lambda_0}\right)^2$
$\lambda < \lambda_0$	Plate members	$\frac{1+0.45(\lambda/\lambda_0)}{1-0.5(\lambda/\lambda_0)^2}$
	Cylindrical members	$\frac{0.87+0.46(\lambda/\lambda_0)+0.12(\lambda/\lambda_0)^2}{1-0.5(\lambda/\lambda_0)^2}$

Note

$$\lambda = l_e\sqrt{\frac{A}{I}}$$

where A is the sectional area of a member, I the moment of inertial of the section of a member, and l_e the effective length of the member

$$\lambda_0 = \sqrt{\frac{2\pi^2 E}{\sigma_y}}$$

where E is Young's modulus and σ_y is the yield stress of material

compressive stress of the ith member, respectively. Mass minimization is critical in the structural design of offshore cranes because it can reduce the overturning moment of a ship. In (18), the design variables (x_i) are the structural dimensions for the cross section of each member (hollow rectangles and tubes for beam elements; solid circles for link elements) as shown in Fig. 7, and their total number is 73. It should be noted that ω_i in (18) is a function of the design variables that are only related to the ith structural member. In this paper, the APDL (ANSYS Parametric Design Language) program was developed to automatically calculate ω_i from the current FE model. SM490YB was chosen as the structural steel because it is primarily used in marine structures. More detailed material properties are listed in Table 4.

In the shape optimization, the following six load cases were used (Cases 1–4 for operation conditions and Cases 5–6 for survival conditions) considering the three-dimensional modeling:

- Case 1: (payload 130.5 tons at the tip of a boom) + (pitch 0.111 rad/s^2) + (heave 2.26 m/s^2)
- Case 2: (payload 130.5 tons at the tip of a boom) + (roll 0.197 rad/s^2) + (heave 2.26 m/s^2)

Table 4 Material properties of SM490YB

Property	Value
Young's modulus	1.206 GPa
Poisson's ratio	0.3
Density	7850 kg/m^3
Yield stress	345 MPa

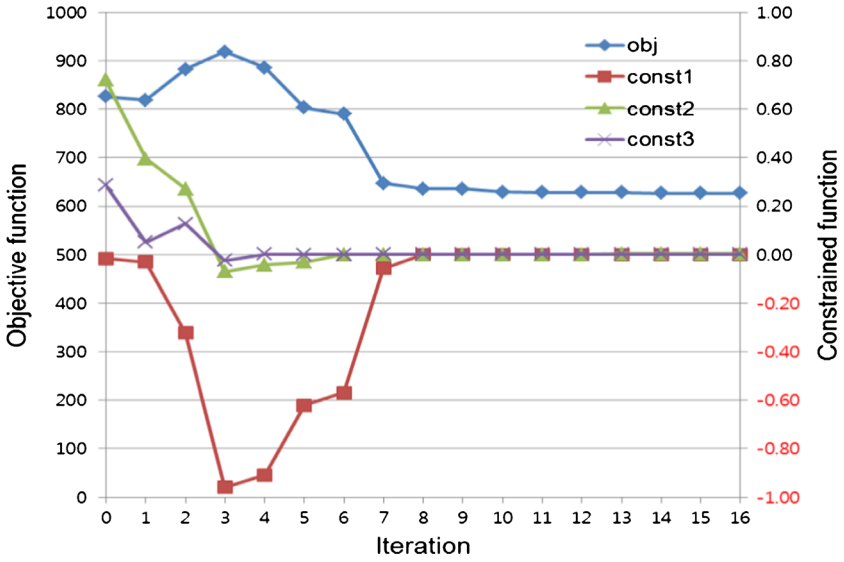

Fig. 8 Optimization history of shape optimization

- Case 3: (payload 130.5 tons at the middle of a boom) + (pitch 0.111 rad/s^2) + (heave 2.26 m/s^2)
- Case 4: (payload 130.5 tons at the middle of a boom) + (roll 0.197 rad/s^2) + (heave 2.26 m/s^2)
- Case 5: (pitch 0.111 rad/s^2) + (heave 2.26 m/s^2) + lateral wind (51.5 m/s)
- Case 6: (roll 0.197 rad/s^2) + (heave 2.26 m/s^2) + head wind (51.5 m/s)

An FEA was performed using BEAM188 and LINK180 in ANSYS for the beam and tension-only members, respectively, and the modified method of feasible directions (MMFD) was used because it is known to be reliable and to use less computer memory. The finite difference method (FDM) with 0.1 % perturbation was used to calculate the sensitivities required in the shape optimization. As shown in Fig. 8, the optimization converged in 16 iterations and took 401 min using an Intel Core i7-950 CPU 3.07 GHz. As a result of the optimization, a mass reduction of 24.1 % was achieved, even from the infeasible design (825.6 tons for the initial design; 626.8 tons for the optimal design). Figure 9 presents the optimized crane design satisfying design regulations. It is should be noted that the quayside crane, which has similar specifications (specifically, lifting capacity 50 tons, rail span 30.5 m, outreach 51 m, and lifting height 34 m), weighs 718.5 tons with SS400 and SM490YB for structural parts.

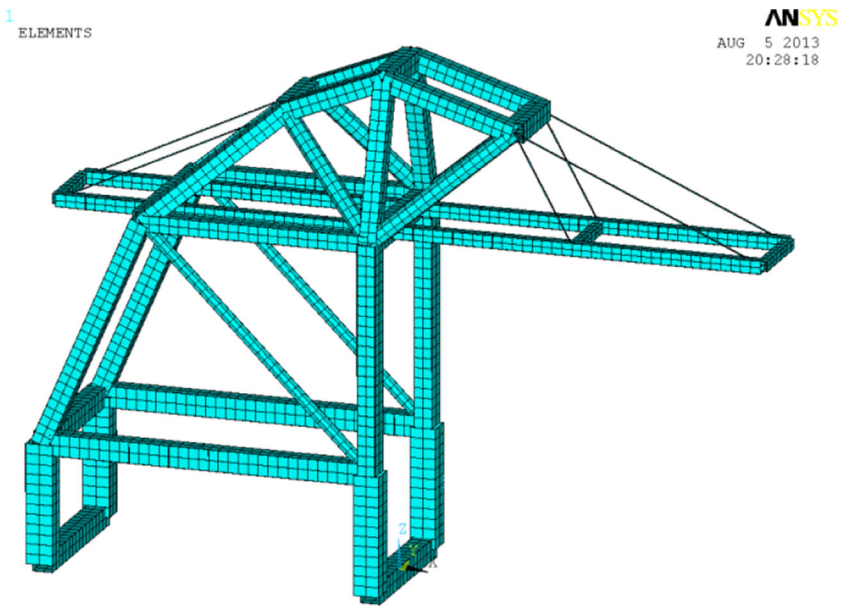

Fig. 9 Optimized Mobile Harbor crane

4 Conclusion

In this paper, a conceptual layout of the Mobile Harbor was proposed with considerations of the design-dependent loads such as self-weight, inertia loads, and wind forces. These forces are essential in appropriately designing Mobile Harbor cranes that operate under open sea conditions. The sensitivities of the design-dependent loads were derived and then applied to the topology optimization under multiple load cases. After obtaining the conceptual design, it was elaborated through shape optimization, which can determine the cross-sectional dimensions required in order to satisfy the design regulations. During the development of the Mobile Harbor, it is essential to reduce the structural mass of the Mobile Harbor crane in order to enhance the overall ship stability. Therefore, the basic design from the mass minimization could successfully achieve this goal. In further research, a similar framework for topology optimization in 3D would be developed in order to obtain a more meaningful conceptual design of the Mobile Harbor and thus propose a better basic design from it.

Acknowledgments This work was supported by the Industrial Strategic Technology Development Program (10036235, Development of the core technology of light weight crane for mobile harbor) funded by the Ministry of Knowledge Economy (MKE, Korea). We would like to thank Dr. Krister Svanberg at KTH (Stockholm, Sweden) for providing the GCMMA code for academic research.

References

Bendsoe MP (1989) Optimal shape design as a material distribution problem. Struct Optim 1:193–303

Bendsoe MP, Kikuchi N (1988) Generating optimal topologies in structural design using a homogenization method. Comput Method Appl Mech Eng 71:197–224

Bruyneel M, Duysinx P (2005) Note on topology optimization of continuum structures including self-weight. Struct Multidiscip Optim 29:245–256

Du J, Olhoff N (2004a) Topological optimization of continuum structures with design-dependent surface loading - part I: new computational approach for 2D problems. Struct Multidiscip Optim 27(3):151–165

Du J, Olhoff N (2004b) Topological optimization of continuum structures with design-dependent surface loading - part II: algorithm and examples for 3D problems. Struct Multidiscip Optim 27(3):166–177

Hammer VB, Olhoff N (2000) Topology optimization of continuum structures subjected to pressure loading. Struct Multidiscip Optim 19:85–92

Hassani B, Hinton E (1998) A review of homogenization and topology optimization I—homogenization theory for media with periodic structure. Comput Struct 69:707–717

James K (2012) Aerostructural shape and topology optimization of aircraft wings. Ph.D. thesis, University of Toronto

Jang IG, Kim IY (2009) Computational simulation of trabecular adaptation progress in human proximal femur during growth. J Biomech 42(5):573–580

Jang IG, Kim IY (2010) Application of design space optimization to bone remodeling simulation of trabecular architecture in human proximal femur for higher computational efficiency. Finite Elem Anal Des 46(4):311–319

Jang IG, Kwak BM (2006) Evolutionary topology optimization using design space adjustment based on fixed grid. Int J Numer Method Eng 66(11):1817–1840

Jang IG, Kwak BM (2008) Design space optimization using design space adjustment and refinement. Struct Multidiscip Optim 35(1):41–54

Kim IY, Kwak BM (2002) Design space optimization using a numerical design continuation method. Int J Numer Method Eng 53:1979–2002

Kim EH, Kwak KW, Kim YK, Kim SH, Kwak BM, Jang IG, Kim KS (2013) Auto-positioning of sliding planes based on virtual force. Int J Control Autom Syst 11(4):798–804

Kim EH, Jung YS, Yu YG, Kwon SW, Ju HJ, Kim SH, Kwak BM, Jang IG, Kim KS (2014) An advanced cargo handling system operating at sea. Int J Control Autom Syst. doi:10.1007/s12555-013-0189-3

KR rule book, www.krs.co.kr/KRRules/KRRules2011/KRRulesE.html

Krog L, Tucker A, Rollema G (2002) Application of topology, sizing, and shape optimization methods to optimal design of aircraft components. In: Proceedings of 3rd Altair UK HyperWorks users conference

Osher S, Sethian JA (1988) Front propagating with curvature dependent speed: algorithms based on Hamilton–Jacobi formulations. J Comput Phys 78:12–49

Park KS, Chang SY, Youn SK (2003) Topology optimization of the primary mirror of a multi-spectral camera. Struct Multidiscip Optim 25:46–53

Pedersen N (2000) Maximization of eigenvalues using topology optimization. Struct Multidiscip Optim 20:2–11

Querin OM, Steven GP, Xie YM (1998) Evolutionary structural optimization (ESO) using a bidirectional algorithm. Eng Comput 15:1031–1048

Stolpe M, Svanberg K (2001) An alternative interpolation scheme for minimum compliance topology optimization. Struct Multidiscip Optim 22:116–224

Svanberg K (2002) A class of globally convergent optimization methods based on conservative convex separable approximations. SIAM J Optim 12:555–573

Wang MY, Wang X, Guo D (2003) A level set method for structural topology optimization. Comput Method Appl Mech Eng 192:227–246

Xie YM, Steven GP (1993) A simple evolutionary procedure for structural optimization. Comput Struct 49:885–896

Yang RJ, Chuang CH (1994) Optimal topology design using linear programming. Comput Struct 52:265–275

Zhang H, Zhang X, Liu S (2008) A new boundary search scheme for topology optimization of continuum structures with design-dependent loads. Struct Multidiscip Optim 37(2):121–129

Zakhama R, Abdalla MM, Gürdal Z, Smaoui H (2010) Wind load modeling for topology optimization of continuum structures. Struct Multidiscip Optim 42(1):157–164